Design optimization of a synchronous reluctance motor based on operating cycle

Design Optimization of a Synchronous Reluctance Motor Based on Operating Cycle

Andrea Credo, Paolo Pescetto

***Abstract* – Synchronous reluctance motors are becoming an interesting solution for drives applications requiring high efficiency. The design of those machines is normally based on the optimization of the motor performance at the rated working point in terms of torque production, torque ripple and efficiency, but in many applications the drive will operate for most of the time at partial load and frequent overload may be required, with a speed not necessarily equal to the rated value. In this work we propose an optimized machine design method to maximize the drive efficiency on the total operating cycle, considering a specific speed and torque profile. Four typical working points are selected, each of them maintained by the machine for a different time in the operating cycle. The obtained machine is compared with the one optimized based on the rated conditions only, showing slightly higher losses on a single working point but an improved efficiency on the global operating cycle.**

***Index Terms*—Synchronous reluctance motor, machine design, optimization, synchronous drives, operating cycle, performance maximization, industrial applications.**

I. NOMENCLATURE

I_{ph}	Phase current	R_i	Position of i rotor barrier
I_{SD}	Inner stator diameter	S_H	Slot height
J_s	Current density	S_W	Slot width
O_{SD}	Outer stator diameter	T_{avg}	Average torque
O_{RD}	Outer rotor diameter	V_{ph}	Phase voltage
p	Pole pairs	X_i	Width of i rotor barrier

II. INTRODUCTION

ACCORDING to [1] the 35%-40% of the generated electrical energy worldwide is consumed by industrial electric motors such as blowers, fans, manufacturing machines, pumps turbines, etc. [2]. Approximately 70% of the industrial electricity is consumed by the electric motor systems, representing the most important type of load in industry. Therefore, the efficiency improvement of electric motors would strongly contribute to reduce the energy consumption and the environmental impact. As claimed by Ferreira in [3] more than 90% of the installed electric motors are three-phase squirrel-cage Induction Motors (IM), mostly because of their cost-effectiveness, robustness and the possibility to be directly fed by the grid. Alternatively, when the application requires a fixed speed a line-start synchronous machine can reach a higher efficiency exceeding the IE4 class [4].

Considering the low power size applications, the efficiency of IMs is typically lower than the one of Synchronous Reluctance motors (SynRel), mostly because of the Joule losses in the rotor cage [5].

Nowadays electrical machines simulation software based on Finite Element Analysis (FEA) are able to accurately compute the machine losses and performances in terms of average torque and torque ripple for a given current vector and the required voltage. An accurate analysis of the machine may require a very fine mesh and a short simulation step-time. Moreover, a post-processing is often necessary for evaluating, as an example, the effect of mechanical tolerances, resulting in considerable computational time. Anyway, the optimization algorithms, simulation software and computational power are constantly improving, permitting a more and more sophisticated representation of the machine and so an optimal machine design in a reasonable simulation time.

The typical motor design procedure requires a geometry optimization. If the motor is designed for a grid supplied application (line starter), the machine will likely work most of the time at its rated speed, correspondent to the grid frequency. In this case, the target of the optimization is normally to maximize the torque and the efficiency at the rated working point. Conversely, since synchronous machines are normally adopted in variable speed drives, a more complex operating cycle profile should be considered, including load and speed variation. This can be done by modifying the machine design algorithm in order to consider different working points within the optimization procedure [6]. In this case, the computational time for the performance evaluation depends on the number of considered working points. For this reason, when the application requires that the machine should work in a high number of different working points there are two possible strategies for the optimization algorithm:

- evaluating the machine performances in a low number of working points (typically 4 or 5) identified to properly represent the working cycle;
- developing an analytical model aided by the FEA to be used for the performance estimation.

The first approach, that will be adopted in this work, is possible thanks to the constant increase of the computational power. In particular, the paper focuses on the optimization of a SynRel motor for an industrial application that works in the duty cycle type S8 (continuous-operation periodic duty with related load/speed). This duty cycle is defined as a repeated sequence of different working points in terms of torque and speed applied for a defined time.

This paper is organized as follows. The machine specifications, the adopted model and variables, and the

A. Credo is with the Department of Industrial and Computer Engineering and Economics, University of L'Aquila, L'Aquila, Italy (e-mail: andrea.credo@graduate.univaq.it).

P. Pescetto is with the Energy department "Galileo Ferraris", Politecnico di Torino, Torino, Italy (e-mail: paolo.pescetto@polito.it).

results of the preliminary design of the SynRel motor are presented in Section III. The proposed optimization procedure is discussed in Section IV. Then, the results and the comparison of the optimizations are shown in Section V. Finally, a summary of the achieved conclusions is given in Section VI.

III. The Synchronous Reluctance Motor

The SynRel motor is often adopted because of its low-cost (thanks to the absence of magnets or rotor windings) and competitive performance in terms of efficiency and power density [7]. Anyway, it presents lower power factor and torque-to-current ratio [8] compared to other solutions (Permanent Magnet Synchronous Machines and IMs). The torque capability of the SynRel is strictly related to the rotor magnetic anisotropy, obtained by optimizing the rotor shape. A very high magnetic saliency can be achieved, obtaining performances compatible with wound field AC motors. Furthermore, the high rotor anisotropy facilitates the use of saliency based sensorless control algorithms [9] at zero and low speed, while flux observers are used in the medium and high speed ranges [10]. In most applications, the sensorless algorithms require the knowledge of machine parameters, and in particular the magnetic self- and cross-saturation characteristics. Such information is often retrieved by self-commissioning techniques [11][12].

In this paper a SynRel motor with fluid shape has been analyzed and optimized for a particular duty cycle. Fig. 1 and Fig. 2 show the adopted design variables for the optimization at the machine design stage.

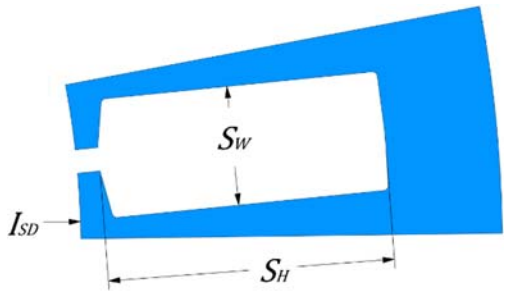

Fig. 1. Stator slot and design variables.

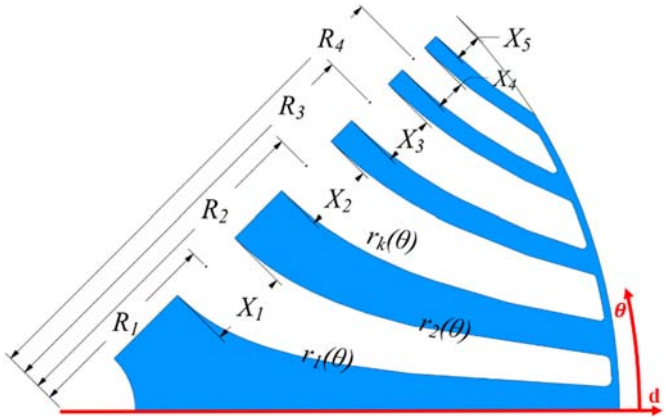

Fig. 2. Fluid-shaped rotor barriers (half pole) and design variables.

In a SynRel, the rotor flux barriers can be designed according to different geometries in order to maximize the torque and minimize the torque ripple. In this work, it was chosen to adopt fluid-shape flux barriers, which guarantee optimal reduction of torque ripple [13]-[15]. The fluid barriers are defined by the following equations:

$$r_k(\theta) = R_S \sqrt[p]{\frac{C_{(k)} + \sqrt{C_{(k)}^2 + 4\sin^2(p\theta)}}{2\sin(p\theta)}} \tag{1}$$

where θ is the mechanical angle with origin in the d axis and $C_{(k)}$ is a constant function of the design variables. For the lower line of the air barrier, $C_{(k)}$ is computed as:

$$C_{(2i-1)}(X_i, R_i) = \frac{\left(\frac{R_i - X_i}{R_s}\right)^{2p} - 1}{\left(\frac{R_i - X_i}{R_s}\right)^{p}} \tag{2}$$

and for the upper line of the air barrier:

$$C_{(2i)}(X_i, R_i) = \frac{\left(\frac{R_i + X_i}{R_s}\right)^{2p} - 1}{\left(\frac{R_i + X_i}{R_s}\right)^{p}} \tag{3}$$

The considered operating cycle for this study is shown in Fig. 3. From this duty cycle it is possible to define four working points:

1. Torque=2.26Nm Speed=4000rpm Time 3.4 min
2. Torque=1.60Nm Speed=6000rpm Time 13.8 min
3. Torque=0.86Nm Speed=8000rpm Time 55.2 min
4. Torque=0.22Nm Speed=8000rpm Time 27.6 min

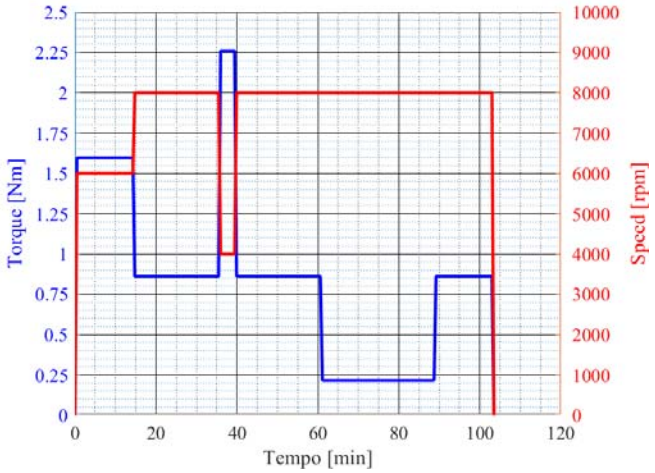

Fig. 3. Duty cycle in terms of torque and speed.

IV. Optimization Method

In this work, the motor geometry has been optimized four times, namely PrD, OPT1, OPT2 and OPT3. In each optimization, the same geometric variables were adopted, but with different constraints and objective functions. Obviously, the common constraint for each optimization is the verification of the torque in each considered working point. The goal of each optimization is:

- PrD: to maximize the machine efficiency at the rated

torque and speed (using analytical expression);

- OPT1: to maximize the global efficiency within the operating cycle;
- OPT2: to maximize the efficiency at the rated point (P2);
- OPT3: to maximize the efficiency at the most frequent working point (P3).

There are many types of optimization algorithm which can require different number of iterations and they can reach different local minimums. The conjugate algorithms are simple in implementation, but they require analytical expression for the objective functions and constraints. The evolutionary algorithms, particle swarm optimization algorithms, estimation of distribution algorithms and genetic algorithm are typically used in the optimization of the electrical machine because they work well coupled with the Finite Element Analysis (FEA) [16]. The used algorithm for the optimization in the manuscript is the derivate free algorithm, considering that the FEA outputs do not include derivative information; it is described in [17]. The used variables for the optimization, their values in the preliminary design, the variability range used in the optimization, the constraints, and the objective functions are shown in Table I.

TABLE I
DESIGN VARIABLES, CONSTRAINTS AND OBJECTIVE FUNCTIONS

Variable	Preliminary	Minimum	Maximum
I_{SD}	77.2mm	68mm	88mm
S_W	5.2mm	4mm	7mm
S_H	12.5mm	9.5mm	15.5mm
X_1	5.5mm	2.5mm	8.5mm
R_1	13.9mm	10.9mm	16.9mm
X_2	4.8mm	1.8mm	7.8mm
R_2	23.6mm	20.6mm	26.6mm
X_3	3.5mm	0.5mm	6.5mm
R_3	29.7mm	26.7mm	32.7mm
X_4	2.1mm	0.5mm	5.1mm
R_4	33.9mm	30.9mm	36.9mm
X_5	1mm	0.5mm	4mm

Optimization	Objective function	Constraint1	Constraint2
PrD	Efficiency (rated)	/	Current density (rated) <4
OPT2	Efficiency (P2)	Torque Ripple (P2) <15%	Current density (P2) <4
OPT3	Efficiency (P3)	Torque Ripple (P3) <15%	Current density (P3) <2.6
OPT1	Efficiency (cycle)	Torque Ripple <15%	Current density (cycle) <4

The slot opening was not included among the optimization variables in order to minimize their number. Despite the slot opening deeply affects the performance of the machine, its minimum value is imposed by manufacturing constraints force its minimum value. Since the slot opening should be small for reducing the torque ripple, the value of the slot opening was chosen as small as possible according to the manufacturing constraints. The maximum current density has been used as constraint in order to obtain a maximum motor temperature compatible with the application. For this reason, the maximum current density in each working point has to be the same for the different optimizations. Therefore, the value of that constraint is different among the optimizations.

The used electrical steel for the application is the commercial steel 470-50A. In the Fig. 4 the magnetization curve (B/H) is presented while Fig. 5 shown the specific losses curve in function of the flux density B at different value of frequency [18].

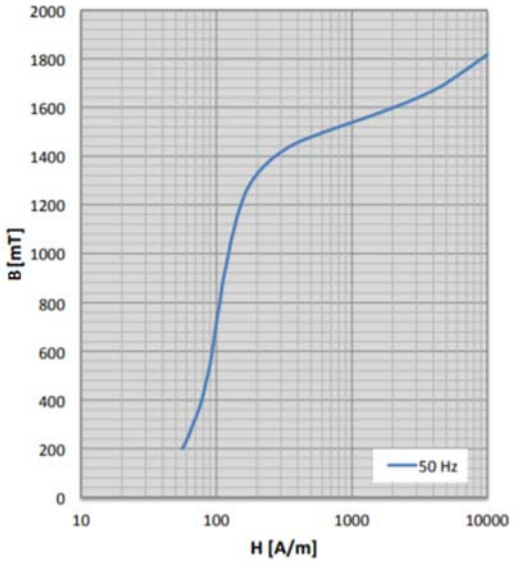

Fig. 4. Characteristics B/H magnetization curve.

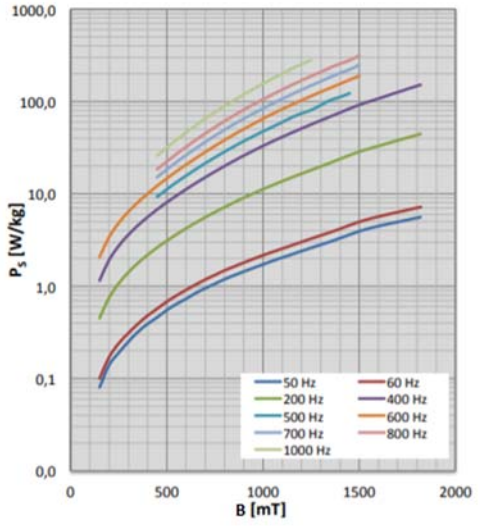

Fig. 5. Characteristics Ps/B specific loss curve.

In the first optimization, a preliminary design (PrD) of the stator core has been conducted using the typical sizing procedure adopted for an induction machine, but considering a lower power factor [19], thus defining the inner stator diameter, the number of conductors in each slot, the rated phase current, and the width and the height of the slots. A similar methodology is used for the calculation of the preliminary design of the rotor core with fluid barriers. The preliminary design is optimized considering the motor torque and speed at rated conditions.

The performance of the machine obtained with the preliminary design (PrD) for the different points of the

operating cycle are indicated in Table II.

TABLE II
PERFORMANCE OF THE PRELIMINARY DESIGN

Working Point	Current [Arms]	Efficiency [%]	Losses [J]
1	50.9	87.06	416.5
2	37.5	91.51	1177.8
3	23.0	93.00	2783.9
4	11.4	91.03	456.3
Cycle	23.9	92.76	4834.5

Fig. 6, Fig. 7 and Fig. 8 show the behavior of the objective functions in the three optimizations OPT1, OPT2 and OPT3. For those points that do not satisfy the constraints, the objective function (machine efficiency) has been forced to 0, thus excluding them for the final design. In the figures the blue dots are the points which satisfy the constraints while the red dots do not satisfy the constraints.

It is worth noting that the optimization OPT1 requires a little bit more iterations to achieve convergence compared to the others and in the initial phase it starts from lower values of the objective function. This is due to the higher number of working points considered in the optimization. The behaviors of the objective functions of the optimizations OPT2 and OPT3 are quite similar because both the optimizations consider only one working point. OPT2 and OPT3 are able to reach a high value of efficiency satisfying all the constraints after only 1000 iterations, while OPT1 needs at least 3000 iterations. The last iterations in all optimizations are necessary to refine the results and to reach the optimal design.

V. COMPARISON BETWEEN THE DIFFERENT OPTIMIZATION STRATEGIES

This Section compares and discusses the results of the geometric optimizations. The four different optimization strategies have been compared in terms of final geometry, level of steel saturation in the machine, efficiency, RMS current, and losses for each working point and in the cycle. The geometry and the induction field are discussed to understand what is the difference between the results obtained from the optimization that considers a single working point and the one considering an operating cycle.

Fig. 9 shows the stator and rotor geometries obtained from the preliminary design and from the other optimizations. Since the project OPT1 considers also the working point P1 (that is the overload of the motor in terms of torque), in order to minimize the losses, the width of the rotor yokes is greater compared to the other designs, thus reducing the saturation level, the phase current and the losses in overload conditions. The project OPT3 has the thinnest rotor yokes because it is optimized considering only the working point P2, characterized by a torque lower than the rated value. Therefore, the current and the losses in the working point P1 of the OPT2 and OPT3 will be much higher than the ones of the OPT1 design. All these considerations are confirmed by the figures of the magnetic flux density in the working points P1 (Fig. 10), P2 (Fig. 11) and P3 (Fig. 12).

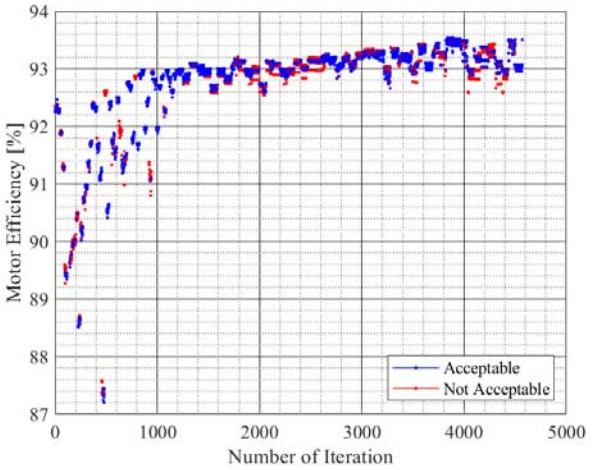

Fig. 6. Behavior of the objective function in the optimization OPT1.

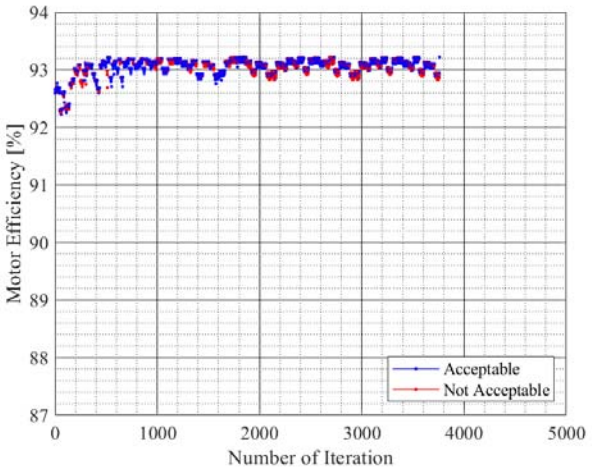

Fig. 7. Behavior of the objective function in the optimization OPT2.

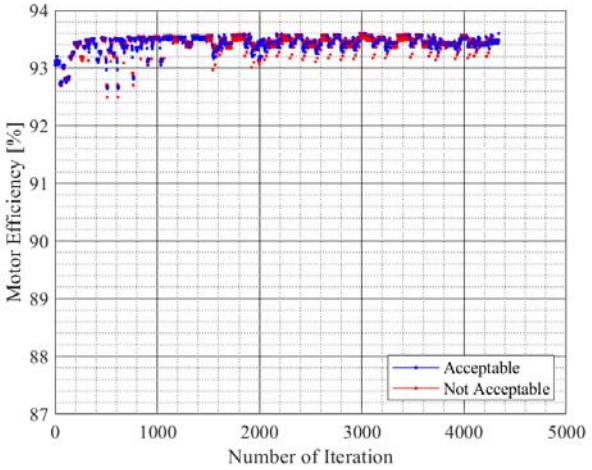

Fig. 8. Behavior of the objective function in the optimization OPT3.

Fig. 10 shows the magnetic flux density of each optimized geometry in the working point P1. OPT1 has the lowest saturation value in the stator yoke and teeth and in the rotor yokes. This results in the best performance in the working point P1 compared to the other projects. The preliminary design has the highest saturation value, while the project

OPT2 presents a magnetic flux density a little bit lower than the one of project OPT3.

Fig. 11 shows that the level of the magnetic flux density in the rotor yokes of the project OPT1 is very low, while the stator yoke and teeth of the project OPT 3 are saturated; these two aspects lead to a lower value of magnetic anisotropy, and thereby to a reduction of the motor torque capability.

Fig. 12 shows the magnetic flux density of each designs for the working point 3. The project OPT3 has the thinnest rotor yokes, but with this current the saturation is not reached, so it presents the highest level of anisotropy. The projects OPT1 and OPT2 have the lowest value of magnetic flux density and they have thinner rotor flux barriers, leading to a lower magnetic anisotropy of the machine.

The results of the optimized designs considering the operating cycle are reported in Table III. The numerical results confirm the analytical considerations based on the study of the induction field and saturation levels.

In particular, the project OPT1 has the lowest current and losses and the highest efficiency for the working point P1 as well as the projects OPT2 and OPT3 considering the working point P2 and P3 respectively. As expected, considering the

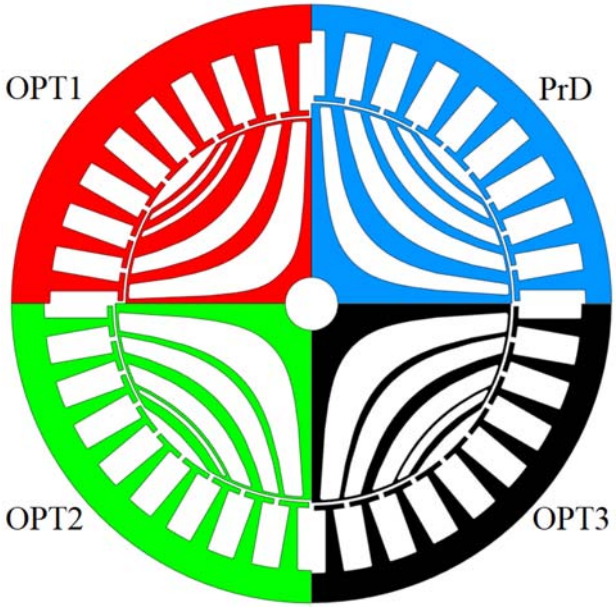

Fig. 9. Stator and rotor geometry of the Preliminary Design (PrD), of the optimization in the cycle (OPT1), in P2 (OPT2) and in P3 (OPT3).

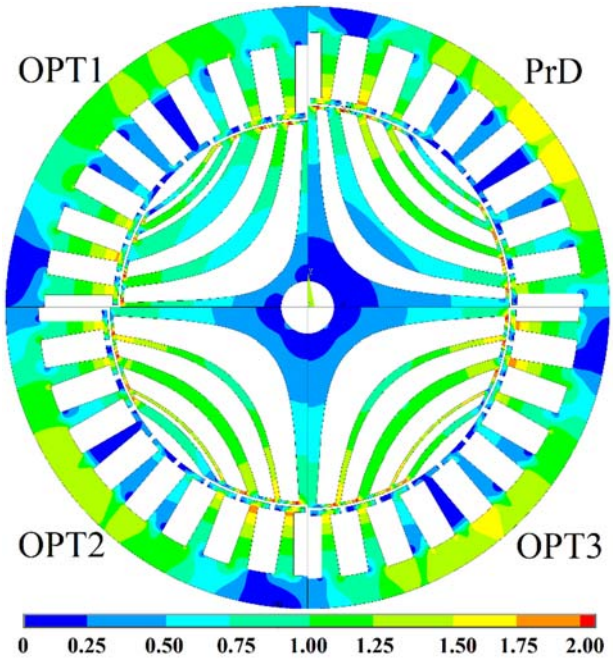

Fig. 11. Magnetic flux density [T] of the Preliminary Design (PrD), of the optimization in the cycle (OPT1), in P2 (OPT2) and in P3 (OPT3) for the working point 2.

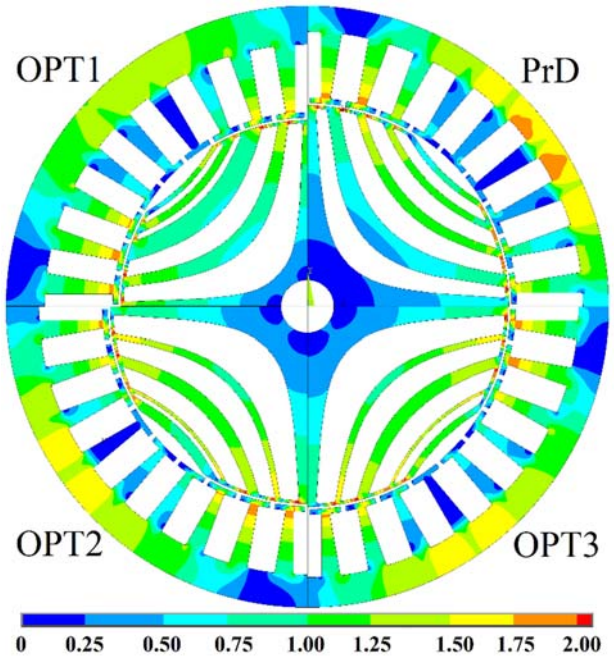

Fig. 10. Magnetic flux density [T] of the Preliminary Design (PrD), of the optimization in the cycle (OPT1), in P2 (OPT2) and in P3 (OPT3) for the working point P1.

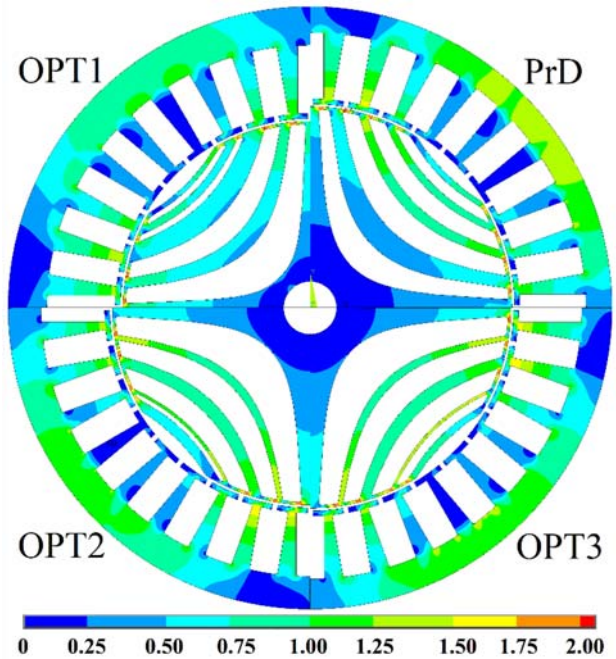

Fig. 12. Magnetic flux density [T] of the Preliminary Design (PrD), of the optimization in the cycle (OPT1), in P2 (OPT2) and in P3 (OPT3) for the working point 3.

operating duty cycle of the machine, the best project is OPT1 that has the highest efficiency. Nevertheless, the design of this optimized geometry requires much more computational time. Alternatively, the results show that the computational time can be reduced, still guaranteeing a good efficiency, by optimizing the motor geometry only considering the most frequent working point instead of the rated one.

TABLE III
PERFORMANCE OF THE OPTIMIZED DESIGNS

	Current [Arms]		
Working Point	OPT1	OPT2	OPT3
1	**39.4**	43.5	45.3
2	32.6	**31.2**	32.3
3	22.5	22.8	**22.4**
4	11.3	11.4	11.3
Cycle	**21.38**	21.52	21.48
	Efficiency [%]		
Working Point	OPT1	OPT2	OPT3
1	**90.83**	89.76	89.37
2	93.06	**93.22**	92.80
3	93.47	93.26	**93.60**
4	91.28	91.11	91.26
Cycle	**93.51**	93.36	93.47
	Losses [J]		
Working Point	OPT1	OPT2	OPT3
1	**295.0**	329.6	342.2
2	962.8	**940.6**	998.9
3	2597.0	2680.5	**2545.3**
4	443.6	452.2	444.6
Cycle	**4298.4**	4402.9	4331.0

To confirm this assert, the optimization that considers all the working points (OPT1) was capable to reduce the losses of the cycle by only ≈30J (increasing the efficiency of ≈0.04%) compared with the project optimized using the most frequent working point (OPT3). Compared to optimized project that only uses the rated point there is a loss reduction of 100J (increasing the efficiency of about 0.15%). In other words, the project OPT1 obtained a loss reduction of 2.43% and 0.76% compared to the projects OPT2 and OPT3 respectively.

Another good feature of the OPT1 is that, since each working point of the duty cycle is considered, it is guaranteed that the value of the torque ripple is within the constraints for every working point. This is normally not automatically guaranteed by the optimizations based on a single working point.

To prove this assert, Fig. 13, Fig. 14 and Fig. 15 show the behavior of the torque in relation to the mechanical angle for all the working points of the project OPT1, OPT2 and OPT3 respectively compared with the torque ripple limits. The figures report all the working points from 1 to 4 from the top to the bottom, respectively. The torque ripple of the project OPT1 for all the working points is lower than the 15%, as imposed by the optimization constraints. When only one point is considered for the optimization (OPT2 and OPT3), the satisfaction of the torque ripple constraint is guaranteed only for the considered working point. Therefore, in the post-processing stage it is necessary to make a further verification of the torque ripple for the other working points. In our case, the projects OPT2 and OPT3 satisfy the constraint of the torque ripple in the point P4, but not for P1.

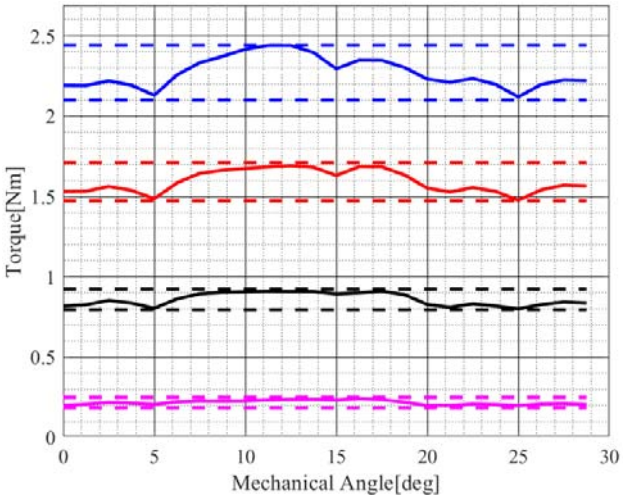

Fig. 13. Behavior of the torque in relation to the mechanical angle for all the working points of the project OPT1.

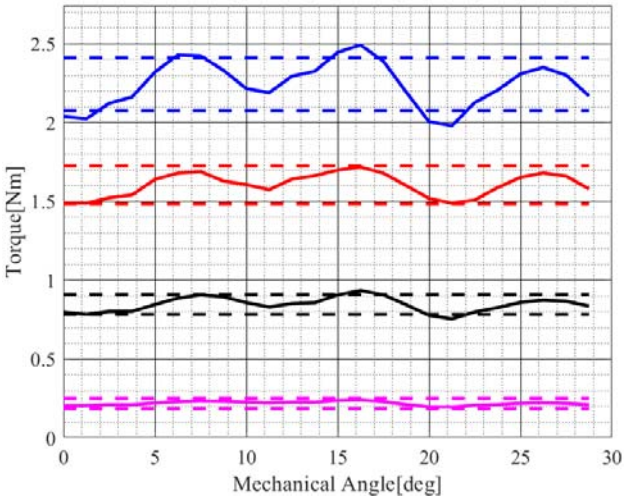

Fig. 14. Behavior of the torque in relation to the mechanical angle for all the working points of the project OPT2.

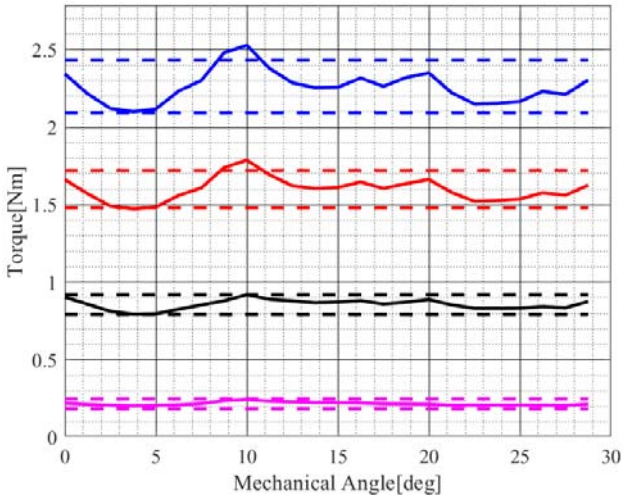

Fig. 15. Behavior of the torque in relation to the mechanical angle for all the working points of the project OPT3.

VI. Conclusion

The adoption of Synchronous Reluctance motors is pushed by the increasing efficiency requirements. For those machines, the typical design strategy assumes the optimization of the motor performance at the rated point, but in most application the motor operates in different torque and speed conditions. If the motor works in a defined operating cycle it is possible to evaluate and optimize the machine geometry in selected representative operative points. The aim of this paper is to optimize the machine considering the full operating cycle and comparing the results for different design optimization strategies. The results have proved that the optimization based on the full operating cycle has a better efficiency, lower losses and phase current, and it guarantees to fulfill the constraints on maximum torque ripple in each operating point, at the cost of a higher computational time. The performance improvement respect to the optimization based on the rated point is higher than the one based on the most frequent point. Future research could examine more complex operating cycle, e.g. typical driving cycle in automotive application, when the torque-speed working points are too numerous to be simulated.

VII. References

[1] A. de Almeida, F. Ferreira and G. Baoming, "Beyond Induction Motors—Technology Trends to Move Up Efficiency", *IEEE Trans. on Industry Applications*, vol. 50, no. 3, pp. 2103-2114, 2014.

[2] R. Saidur, "A review on electrical motors energy use and energy savings", *Renewable and Sustainable Energy Reviews*, vol. 14, no. 3, pp. 877-898, 2010.

[3] F. Ferreira, G. Baoming and A. de Almeida, "Reliability and Operation of High-Efficiency Induction Motors", *IEEE Trans. on Industry Applications*, vol. 52, no. 6, pp. 4628-4637, 2016.

[4] H. Liu and J. Lee, "Optimum Design of an IE4 Line-Start Synchronous Reluctance Motor Considering Manufacturing Process Loss Effect", *IEEE Trans. on Ind. Electronics*, vol. 65, no. 4, pp. 3104-3114, 2018.

[5] M. Villani, M. Tursini, M. Popescu, G. Fabri, A. Credo and L. Di Leonardo, "Experimental Comparison Between Induction and Synchronous Reluctance Motor-Drives," *2018 XIII International Conference on Electrical Machines (ICEM)*, Alexandroupoli, 2018, pp. 1188-1194.

[6] E. Carraro, M. Morandin and N. Bianchi, "Optimization of a traction PMASR motor according to a given driving cycle," *2014 IEEE Transportation Electrification Conference and Expo (ITEC)*, Dearborn, MI, 2014, pp. 1-6.

[7] S. Ferrari and G. Pellegrino, "FEA-Augmented Design Equations for Synchronous Reluctance Machines," *2018 IEEE Energy Conversion Congress and Exposition (ECCE)*, Portland, OR, 2018, pp. 5395-5402.

[8] N. Bianchi, E. Fornasiero, M. Ferrari and M. Castiello, "Experimental comparison of PM assisted synchronous reluctance motors," *2014 IEEE Energy Conversion Congress and Exposition (ECCE)*, Pittsburgh, PA, 2014, pp. 4499-4506.

[9] A. Yousefi-Talouki, P. Pescetto, G. Pellegrino and I. Boldea, "Combined Active Flux and High-Frequency Injection Methods for Sensorless Direct-Flux Vector Control of Synchronous Reluctance Machines," in *IEEE Trans. on Power Electronics*, vol. 33, no. 3, pp. 2447-2457, March 2018.

[10] M. Tursini, M. Villani, G. Fabri, S. Paolini, A. Credo and A. Fioravanti, "Sensorless control of a synchronous reluctance motor by finite elements model results," *2017 IEEE International Symposium on Sensorless Control for Electrical Drives (SLED)*, Catania, 2017, pp. 19-24.

[11] M. Hinkkanen, P. Pescetto, E. Mölsä, S. E. Saarakkala, G. Pellegrino and R. Bojoi, "Sensorless Self-Commissioning of Synchronous Reluctance Motors at Standstill Without Rotor Locking," in *IEEE Transactions on Industry Applications*, vol. 53, no. 3, pp. 2120-2129, May-June 2017.

[12] P. Pescetto and G. Pellegrino, "Sensorless magnetic model and pm flux identification of synchronous drives at standstill," *2017 IEEE International Symposium on Sensorless Control for Electrical Drives (SLED)*, Catania, 2017, pp. 79-84.

[13] R.R. Mpghaddam, “Synchronous Reluctance Machine (SynRM) in Variable Speed Drives (VSD) Applications,“ Ph.D dissertation, The Royal Institute of Technology (KTH), Stockholm, Sweden, 2011.

[14] A. Credo, M. Villani, M. Popescu and N. Riviere, "Synchronous reluctance motors with asymmetric rotor shapes and epoxy resin for electric vehicles," *2019 IEEE Energy Conversion Congress and Exposition (ECCE)*, Baltimore, MD, USA, 2019, pp. 4463-4469

[15] M. Pohl and D. Gerling, "Analytical Model of Synchronous Reluctance Machines with Zhukovski Barriers," *2018 XIII International Conference on Electrical Machines (ICEM)*, Alexandroupoli, 2018, pp. 91-96,

[16] G. Lei, J. Zhu, Y. Guo, C. Liu and B. Ma, "A Review of Design Optimization Methods for Electrical Machines", Energies, vol. 10, no. 12, p. 1962, 2017.

[17] A. Credo, A. Cristofari, S. Lucidi, F. Rinaldi, F. Romito, M. Santececca, M. Villani, "Design Optimization of Synchronous Reluctance Motor for Low Torque Ripple", AIRO Springer Series, pp. 53-69, 2019.

[18] https://www.voestalpine.com/division_stahl/content/download/34047/362537/file/DS%20isovac%C2%A9%20470-50%20A.pdf

[19] I. Boldea, S. A. Nasar, “The induction machines design handbook”, CRC Press, Taylor & Francis Group, 2010.

VIII. Biographies

A. Credo was born in L'Aquila, Italy, in November 1993. He is an Electrical Engineer graduated with honor at the University of L’Aquila in July 2017. He has started his Ph.D. studies in University of L'Aquila in 2017. His main interests are focused on design, modelling and control of electrical rotating machines, with emphasis on automotive applications.

P. Pescetto (S’16 – M’19) received the B.Sc. and M.Sc. degrees with full grade and honors from Politecnico di Torino, Turin, Italy, in 2013 and 2015. Since 2015 he worked in the same institution toward the PhD degree obtained "Cum Laudem" in 2019. Since fall 2019 he is working as researcher in the Energy Department of Politecnico di Torino. He is a member of the Power Electronics Innovation Center (PEIC) of Politecnico di Torino. In 2014 he was an Erasmus Student at the Norwegian University of Science and Technology, Trondheim. He authored or co-authored 10 IEEE journal papers. His main research interests include synchronous motor drives, sensorless control, self-commissioning techniques and integrated battery chargers for EVs. Dr. Pescetto received three Paper Awards in the IEEE conferences and one PELS PhD thesis award.